A&A 401, 1131–1142 (2003)
DOI: 10.1051/0004-6361:20021891

Astronomy & Astrophysics

A transient event in lines of Ne V, VI and VII

E. R. Houdebine[1] and C. Jordan[1]

Department of Physics (Theoretical Physics), Oxford University, 1 Keble Road, Oxford OX1 3NP, UK
e-mail: erh@thphys.ox.ac.uk; cj@thphys.ox.ac.uk

Received 18 September 2002 / Accepted 20 December 2002

Abstract. We report observations of a transition region brightening made with the Coronal Diagnostic Spectrometer onboard the Solar and Heliospheric Observatory. We observed a region of the quiet Sun in 12 spectral lines with temperatures of formation from $\simeq 3 \times 10^4$ K to 1.1×10^6 K. The transient event occured in a network boundary region and was most pronounced in the Ne VI 562.8-Å line. Although the Ne V 572.3-Å and Ne VII 561.7-Å lines also show increases in intensity, the changes in the lines of helium, oxygen and magnesium, formed at lower or higher temperatures, are smaller or not significant. Thus the event is most significant in the relatively narrow temperature range of $\simeq 3 \times 10^5$ K to $\simeq 5 \times 10^5$ K. The event lasted at least 53 min. In the many data sets we have obtained, only one other region shows an obviously high Ne VI to O IV intensity ratio, so the observed event is clearly unusual. Previous studies of blinkers have not included the lines of Ne V, Ne VI or Ne VII; the highest temperature transition region line used has been the O V 627.9-Å line. Future studies of blinkers should include these higher temperature lines. We derive volume emission measures in the event from the various line intensities, estimate the electron densities and discuss the energy budget and possible origins of the event.

Key words. Sun: transition region – Sun: activity – Sun: UV radiation

1. Introduction

The solar atmosphere, and in particular the transition region and the corona, is subject to frequent transient events which may be related to magnetic reconnection. For example, using observations made with the Coronal Diagnostic Spectrometer (CDS) on the Solar and Heliospheric Observatory (SOHO), Harrison et al. (1999) estimated that 3000 blinkers are in progress on the solar surface, at any one time. Blinkers are transient events that have been observed in transition region lines such as O IV 554 Å and O V 630 Å, with little or no increase at the higher or lower temperatures represented by the lines of Mg IX and He I (Harrison 1997; Harrison et al. 1999; Brković et al. 2001; Teriaca et al. 2001). They show a range of durations, depending on the line observed. The typical lifetime is ~17 min, but the average duration is ~40 min. The increase in intensity is usually modest, a factor of 1.5 on average, but in extreme cases may reach a factor of 5 times the pre-event value (Harrison et al. 1999). The average size in O V is $\sim 2.4 \times 10^7$ km^2 (Brković et al. 2001). Blinkers primarily occur in supergranulation network boundaries.

Transient brightenings have also been observed at other wavelengths and temperatures; Berghmans et al. (1998) observed the quiet Sun at extreme ultraviolet wavelengths with the SOHO Extreme Ultraviolet Imaging Telescope (EIT). They observed the He II line at 304 Å and the Fe XII coronal line at 195 Å, with a cadence of one minute. Their analysis of several hours of data revealed many sporadic subflare brightenings and they suggest that the He II band brightenings are equivalent to the blinker events in the oxygen lines reported by Harrison (1997) and Harrison et al. (1999). Berghmans et al. (1998) reported a total blinker birth rate of 20–40 s^{-1}, significantly higher than the rate of 1.24 s^{-1} found by Harrison et al. (1999).

Berghmans et al. (1998) also observed the Fe XII coronal line. They observed brightenings at this wavelength which they refer to as coronal events and liken to the network flares reported by Krucker et al. (1997) and Benz & Krucker (1998). They give a global birth rate at these temperatures of 1.2 s^{-1}, over a factor of ten lower than for the He II events.

Explosive events, discovered by Brueckner & Bartoe (1983), differ from blinkers in that they show larger line widths and sometimes large outflows (see Madjarska & Doyle 2002 and references therein). In ultraviolet spectra they are simultaneously apparent in lines formed between $\simeq 2 \times 10^4$ K and $\simeq 2 \times 10^5$ K. Winebarger et al. (2002) have extended this temperature range through observations of explosive events in the O VI (1032-Å) and Ne VIII (770-Å) lines, formed at around 3×10^5 K and 6×10^5 K, respectively. The relationship between the transient events observed at different temperatures, and between blinkers and explosive events, is not yet clear, but has been discussed by Chae et al. (2000). Further observations

Send offprint requests to: E. R. Houdebine,
e-mail: erh@thphys.ox.ac.uk

over a broad range of temperatures and a large area of the Sun are required in order to elucidate these points.

Here we report observations of the quiet Sun made with the CDS on SOHO using Joint Observing Programme (JOP) 62. JOP 62 includes lines which are formed over the temperature range from $\simeq 3 \times 10^4$ K to 1.1×10^6 K, as used in our previous studies of the helium line enhancements (Macpherson & Jordan 1999; Jordan et al. 2001). We observed a transient network brightening which is strongest in the Ne VI-562.8 Å line and which lasted for at least 53 min. In previous studies of blinkers, the highest temperature transition region line observed was O V (630) Å. We observe a smaller brightening in this line, and even less in other lines of oxygen, and no significant changes in the lines of Mg IX and Mg X. It appears that we have observed a new, and probably rare, type of event, since examination of our previous JOP 62 data sets shows only one region in which the Ne VI/O IV intensity ratio is obviously higher than usual. Our data sets were not designed to look for blinkers, but we can say that the large majority of regions that appear as bright regions in the lines of oxygen also show emission in Ne V and Ne VI. Studies of blinkers should include these lines to cover a wider range of temperatures.

The observations and data reduction are presented in Sect. 2. The properties of the event are described in Sect. 3. The plasma parameters and interpretation are discussed in Sect. 4. Section 5 presents our conclusions.

2. Observations and data reduction

The observations were obtained with the CDS instrument on SOHO on 2001 May 15 and 16. The transient event was observed in the data set obtained on May 16. The SOHO satellite and the CDS instrument are described by Domingo et al. (1995) and Harrison et al. (1995), respectively. We observed a region of the Sun near the west limb, centred on solar-X, -Y = 858.4″, 4.4″. The region contains quiet areas, but lies between two active regions, to the north-east and south. Our observing program is a development of the JOP 62 program (see Macpherson & Jordan 1999). It consists of an observing sequence designed for SUMER (Solar Ultraviolet Measurements of Emitted Radiation) and CDS. The details of the CDS observing sequence are given in Table 1, together with some of the parameters of the observations. Our observations made with SUMER do not include the location of the transient event and are not discussed here.

We used the normal incidence spectrometer and detectors NIS 1 and 2, which cover the wavelength regions 308–381 Å and 513–633 Å. The observing seqence includes 15 spectral windows. The wavelengths of the lines used and the temperatures at which each line has its maximum emissivity are given in Table 2.

The slit used had an area of 2 × 240 arcsec^2. Rastering in the X direction for 20 exposures covers an area of 40 × 240 arcsec^2. This ensures the inclusion of supergranulation cell boundaries and interiors. The pixel size corresponds to 2 arcsec (the slit-width) by 1.67 arcsec, in solar-X and -Y, although the spatial resolution achieved in practice is probably lower. Scanning the smallest bright area in the field of view gives a full-width at half maximum ($FWHM$) of 4.8 arcsec in the Y-direction. The width of each spectral window was fixed at 30 pixels, which corresponds to ≃3.4 Å. This allows checks on the presence of blends, ensures that the complete line profiles are included and also allows the background flux on either side of a spectral line to be estimated.

Table 1. Details of the CDS observing sequences. The duration of the observations includes dead-time between exposures.

Instrument	CDS-NIS 2
Slit size	2 arcsec × 240 arcsec
Exposure time	70 s
Window size	30 pixels (≈3.4 Å)
No. of spectral windows	15
No. of exposures/raster	20
No. of rasters	4
Raster area	40.6 × 240.2 arcsec^2
Duration of observations	106.2 min
Solar X, Y (centre)	858.4″, 4.4″
Start times of	06:49:48.3, 07:16:25.6
observations	07:42:59.8, 08:09:34.8
Date of observations	2001 May 16

The CDS data were reduced with the analysis software available from the SolarSoft software package. This software provides tools for reducing and analysing the CDS FITS files. The data were reduced following the standard procedure (see e.g. Macpherson & Jordan 1999).

There can be a spatial offset between the two detectors NIS 1 and NIS 2, which can amount to several arcseconds in the N/S direction. In the present observations only the Mg IX 368.07-Å line is observed with NIS 1. By comparing the images in the Mg IX line and in the lines observed with NIS 2, we find that, relative to the Mg X image, the Mg IX image is offset to the south by ≃8 arcsec.

We have used the V4 calibration in measuring the line intensities. The original CDS_NIS 2 calibration was obtained from the preliminary report on the CDS laboratory calibration by Bromage et al. (1996). Further analyses based on differential emission measures were made by Landi et al. (1997), and in our previous work (Macpherson & Jordan 1999; Jordan et al. 2001) we adopted their proposed calibration. Later, the calibration was revised according to the work of Brekke et al. (2000), who compared simultaneous observations using NIS and the NASA/LASP EUV Grating Spectrometer experiment. In Jordan et al. (2001) we also gave the factors to convert to the calibration by Brekke et al. (2000). The most important difference between the current calibration and that by Landi et al. (1997) is the second-order correction factor for the He II 304-Å line, which is now a factor of ≃26, not 55. Otherwise, the V4 calibration gives an overall increase in the sensitivity which leads to lower intensities.

The line profiles have changed since the recovery of SOHO (see CDS software note No. 53). The spectral resolution is now lower and this makes the extraction of the intensities of blended lines more difficult. For unblended lines the line intensities were measured using the CDS software which makes fits

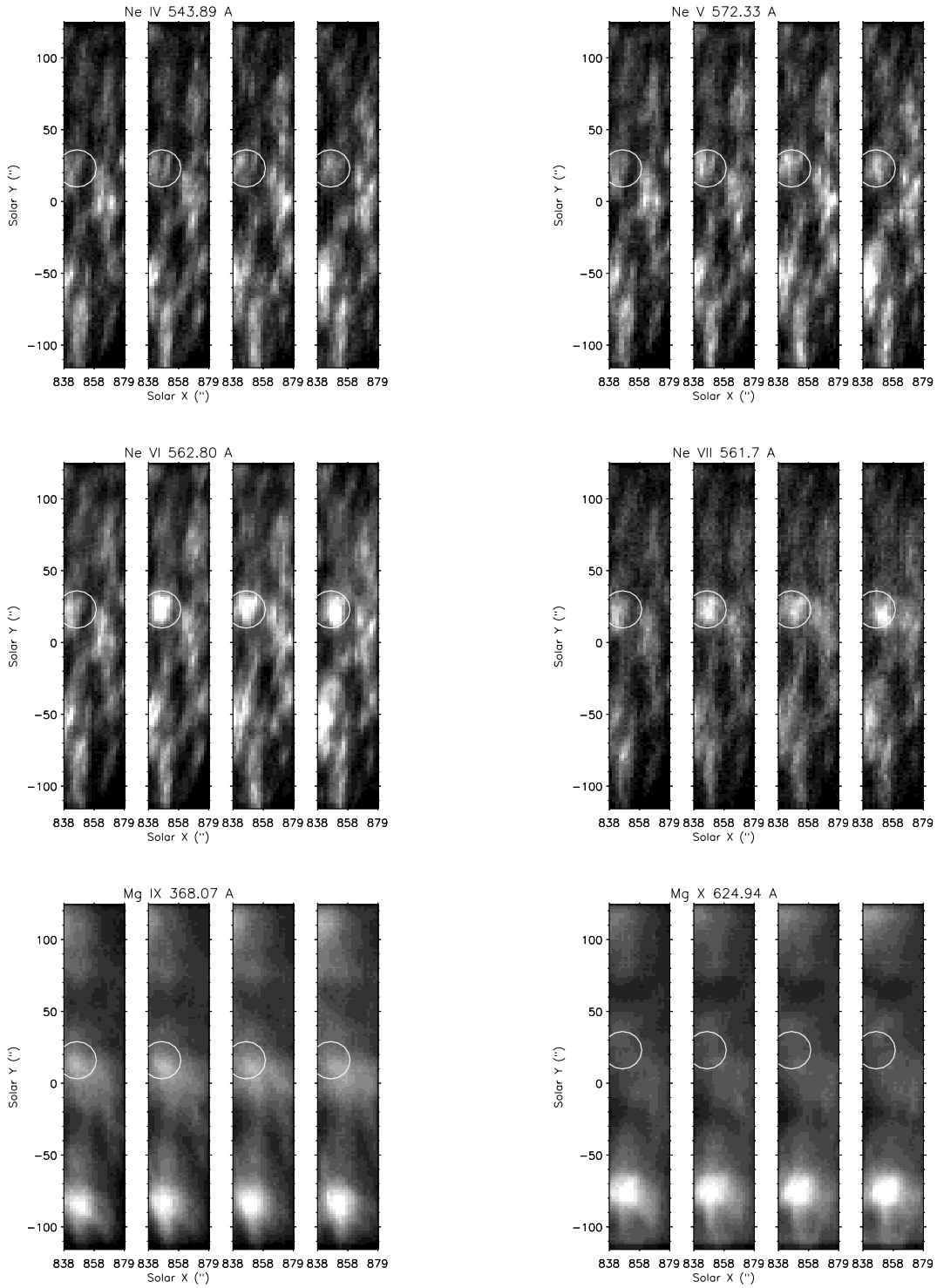

Fig. 1. Rasters made in the Ne IV (543.9-Å), Ne V (572.3-Å), Ne VI (562.8-Å), Ne VII (561.7-Å), Mg IX (368.1-Å) and Mg X (624.9-Å) lines. The mid-times of the observations are (from left to right in each panel) UT 07:03:01, 07:29:37, 07:56:12 and 08:22:47. A brightening is clearly apparent in the Ne VI and Ne VII lines, within the superposed area (of diameter 30 arcsec, centred at solar-X, -Y = 847″, 23″). This brightening is less obvious in Ne IV and Ne V. No significant changes occur in Mg IX or Mg X. Note that the Mg IX rasters are offset in solar-Y by 8 arcsec to the south, relative to the lines observed with NIS 2.

to the profile taking account of the instrumental profile. Where such fits were not possible the intensities were found by integrating over a chosen wavelength region, taking into account the background. The total intensity in the O IV multiplet around 554 Å was measured.

3. Properties of the transient event

3.1. Spatial behaviour

Figure 1 shows the rasters in the Ne IV, Ne V, Ne VI, Ne VII, Mg IX and Mg X lines for the four successive exposures

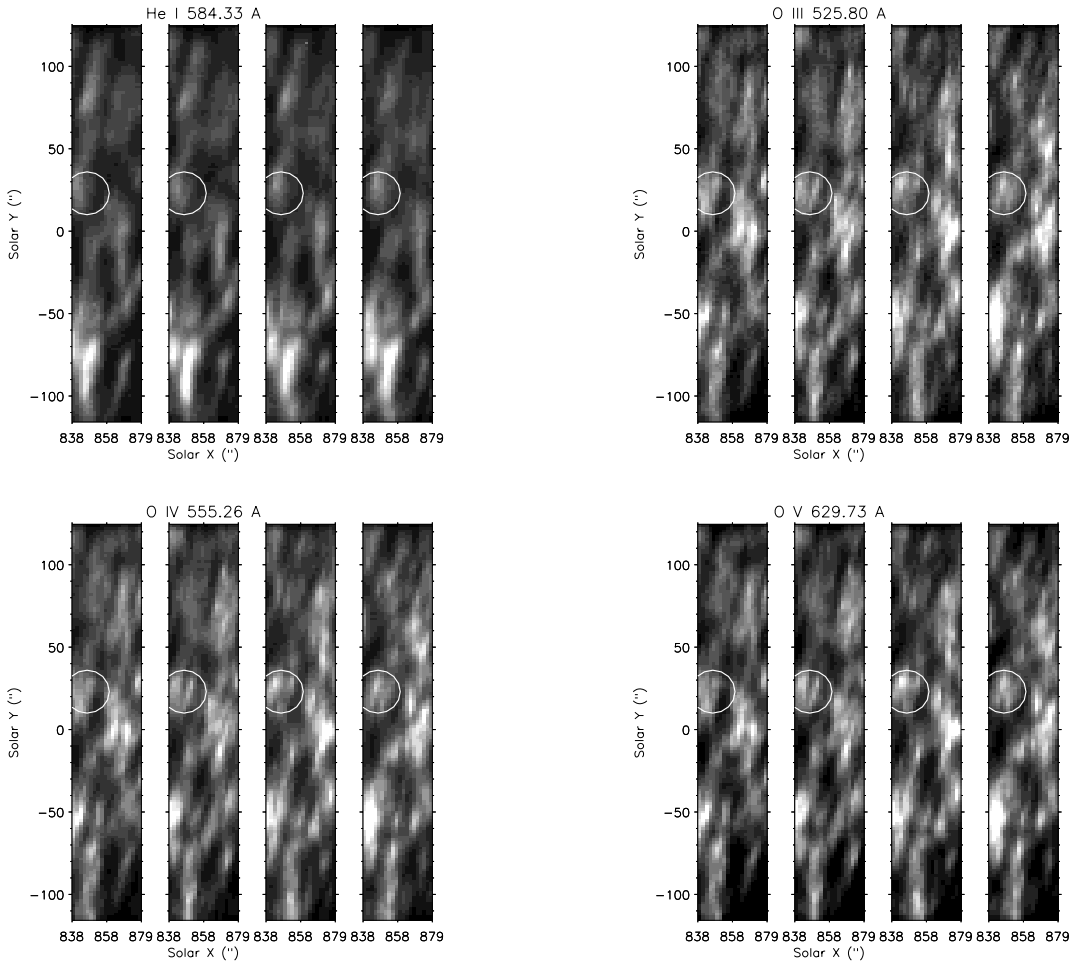

Fig. 2. Rasters in the He i (584.3-Å), O iii (525.8-Å), O iv (554-Å) and O v (629.7-Å) lines. (See Fig. 1 for times.) The significant brightening in the Ne vi and Ne vii lines, apparent in Fig. 1, is not observed in the lines shown here.

taken at UT 07:03:01, 07:29:37, 07:56:12 and 08:22:47 on 2001 May 16 (mid-times of the observations). Solar rotation causes displacements of ≃2 arcsec between successive rasters. The area superimposed has a diameter of 26 arcsec and is centred on solar-X, -Y = 847″, 23″. This set of lines shows the changes in the structures present at temperatures between $\log T_e = 5.27$ and 6.04 (see Table 2 for optimum temperature for the formation of each line). In the quiet atmosphere, the Ne iv and Ne v lines are formed in the mid-transition region, those of Ne vi and Ne vii are formed in the upper transition region and those of Mg ix and Mg x are formed in the high transition region/lower corona.

The first image of each set (UT 07:03:01) shows the typical bright and dark regions corresponding, respectively, to supergranulation boundaries and cell interiors and also an active region at solar-Y below ≃ −60″. In the lines of Ne iv to Ne vi there is nothing particularly unusual about the encircled area. In the Ne vii line this region tends to be brighter than average, for areas outside the active region.

In the second image of each set (UT 07:29:37), a bright region appears in the Ne vi line centred at about solar -X, -Y = 847″, 23″. This feature has an extent of δX, $\delta Y \approx 12$ arcsec, 18 arcsec, which represents ≈8 700 km by 13 000 km on the Sun. The brightening is also clearly visible in the Ne vii line, but is not centred at precisely the same location, being offset by about 3 arcsec to the southwest. Similar small differences in position are visible between the two lines in the third and fourth images of each set (UT 07:56:12 and 08:22:47). The apparent changes with time in the position in the solar-X direction are consistent with those expected from the solar rotation rate near the equator (Allen 1973). However, in the fourth images the brightening in Ne vi and Ne vii appears to have moved by about 3 arcsec to the south and the emission is also more concentrated in area compared with that in images 2 and 3. In the lines of Ne iv and Ne v, throughout exposures 2, 3 and 4, the encircled region is not remarkably unusual compared with other boundary regions; if the lines of Ne vi and Ne vii had not been observed, there would be no evidence that any unusual event had taken place.

The Mg ix images show a more extended bright region centred on solar-X, -Y = 846″, 20″ (after the offset of 8 arcsec in solar-Y between the NIS-1 and NIS-2 images has been applied). Thus the Mg ix region is offset from the Ne vi bright region by ≃3 arcsec to the south. The changes in the Mg ix emission are of only marginal significance (see Sect. 3.2). Similarly, the Mg x image shows little variation.

Figure 2 shows the rasters obtained in the lines of He i, O iii, O iv and O v. In the region of the strong Ne vi emission, there

Table 2. Lines observed in the CDS sequences, which have sufficient intensity for useful analyses.

Ion	$\log T^a_{\max}$	Detector	Wavelength[b] (Å)
He I	4.5	NIS 2	584.33
			537.03
He II	4.9	NIS 2	303.78 (2nd ord.)
O III	5.05	NIS 2	599.60
O IV	5.27	NIS 2	553.33
			554.08
			554.51
			555.26
O V	5.38	NIS 2	629.73
Ne IV	5.27	NIS 2	543.89
Ne V	5.45	NIS 2	572.11 bl
			572.34 bl
Ne VI	5.63	NIS 2	562.71 bl
			562.80 bl
Ne VII	5.72	NIS 2	561.38 bl
			561.73 bl
Mg IX	5.97	NIS 1	368.07
Mg X	6.04	NIS 2	624.95

[a] The temperature at which the line emissivity peaks using ion populations of Arnaud & Rothenflug (1985).
[b] Wavelengths are taken from Kelly (1987). Unresolved blends are indicated by bl.

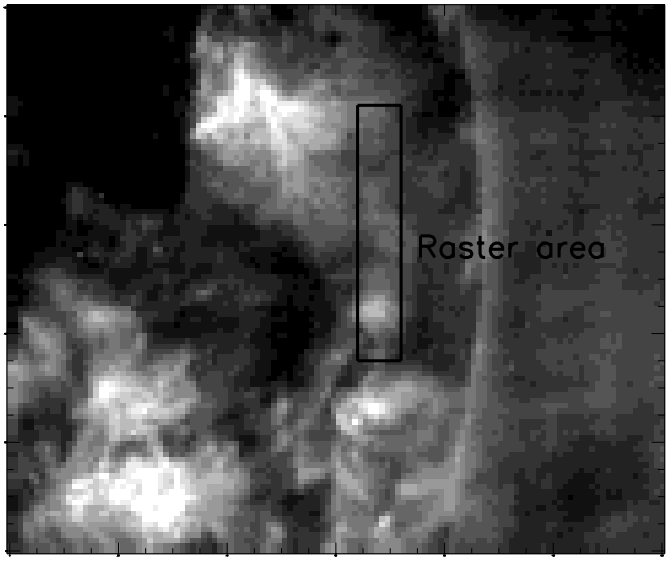

Fig. 3. The EIT image in Fe XII (195 Å) taken at UT 07:25:37 on 2001 May 16. The location of the region rastered with CDS is shown. North is up.

are only small changes in the He I emission. The small changes in the pattern of the emission in the oxygen lines are very similar to those in the Ne IV line. In particular, there are no significant differences between the images in the Ne IV and O IV lines, which are formed at essentially the same temperature.

A series of EIT images in the Fe XII 195-Å line is available throughout the time of our observations. Over the area of interest, no changes are apparent in the Fe XII emission. In Fig. 3 we show the EIT image recorded at UT 07:25:37, during our second raster images. The location of the area rastered with the CDS is also shown. The bright patch associated with the small active region to the south is apparent in both the EIT and CDS images.

3.2. Intensities

In raster 1, over the area covered by solar-X from 841.5 to 854.8″ and solar-Y from 7.8 to 33″ (to include the boundary region in which the brightening later takes place), the average intensities of the transition region lines formed up to the temperature of Ne V are about a factor of 2 larger than those measured by Macpherson et al. (1999) in the "normal" boundaries at Sun-centre (allowing for the changes in calibration). In a plane-parallel layer, the limb brightening would be about a factor of 2 at the longitude of our observations. Thus the boundary region in which the brightening takes place appears to be fairly typical.

The observation of the Ne VI brightening in three consecutive images (rasters 2, 3 and 4) implies that the enhanced emission in this line has been sustained for at least 53 min. To illustrate the changes in the intensity of the Ne VI line, we subtracted the first Ne VI image from the subsequent images, shifting the position of the first image to account for the solar rotation. The results are shown in Fig. 4. The increase in the Ne VI line in raster 2 (within the encircled region) is clearly apparent, as are the changes in the location of the largest enhancements in rasters 3 and 4. There are changes in other network regions, and in the active region to the south, but none is as large in area and as intense as the region under study. Outside of the active region these changes could be related to blinkers. Difference images in other lines (e.g. of O III, IV and V) also show these blinker-like changes, but do *not* show increases in the region where the Ne VI and Ne VII lines are enhanced.

We have also examined regions where the line intensities *decrease* with time. Although such regions can be seen in Figs. 1 and 2, the difference images do not show systematic behaviour which can be related to the location where the Ne VI and VII lines increase.

Since many small changes in the Ne VI intensity occur, to emphasize further the unusual nature of the region of interest, we show in Fig. 5 the ratio of the Ne VI line to the Ne IV line as a function of position, in all four exposures (in the order, top left to right, then bottom, left to right). The most important point is that none of the other regions where there are increases in the Ne VI line (see Fig. 4) have such large Ne VI to Ne IV intensity ratios. Comparisons are made with Ne IV as its behaviour is typical of the mid-transition region lines. Because the lines are relatively weak, and the noise in the ratio is quite high, we have *not* subtracted the background emission in producing Fig. 5, so the scale of the intensity ratios should not be used. The first raster shows a flat (but noisy) image with a possible small enhancement in the north-west end corner, showing that the ratio of the two lines is essentially constant over the cell boundaries and interiors, and in the active region to the south. In the other

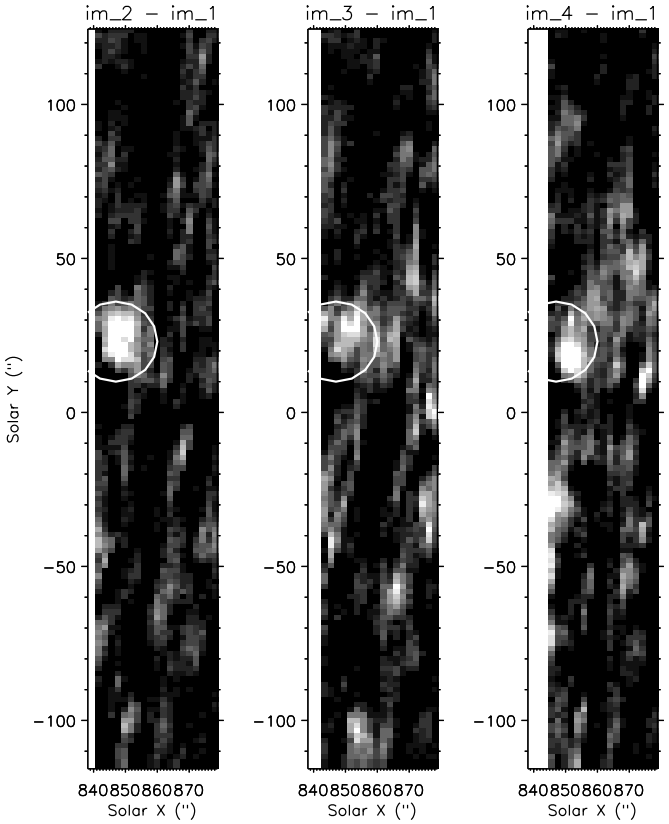

Fig. 4. Images obtained by subtracting the intensities of the Ne vi (562.8-Å) line in the first raster from those in rasters 2, 3 and 4, allowing for solar rotation. These show the brightening centred on solar-X, -Y = 847″, 23″ (in raster 2) and the changes in location of the strongest brightening. In the second image, the largest change is in the northern part of the patch, while in the third image the strongest brightening has shifted to the south.

rasters a substantial increase in the ratio can be seen at the location of the Ne vi brightening discussed above. A decrease in the ratio in the third raster and the subsequent increase in the fourth image is apparent. There are changes in the spatial variation of the high ratios; the sharp peak in the second and fourth images is not present in the third image. In the second and fourth images the ratio increases steadily from the edges to the centre of the region.

When the intensities are corrected for the background emission, most of the Ne vi to Ne iv intensity ratios are concentrated around a value of 1.5, irrespective of the intensity of the Ne iv line. In rasters 2, 3 and 4 there is also a group of points which have significantly larger ratios, which reach to a maximum value of 6. These high values of the ratio occur at Ne iv intensities which are typical of network boundaries. The small range of the intensity ratio over the major part of the rasters shows that the *shape* of the emission measure distribution between 1.9×10^5 K and 4.4×10^5 K is very similar in all regions not associated with the brightening. (See Jordan et al. 2001, for similar results over other temperature ranges, and Jordan 2000 for the implications in terms of the energy balance).

To demonstrate the quantitative variations in the line intensities we have first measured the total intensities in raster 1, over an area of 66 pixels^2 (corresponding to solar-X = 840.5 to 850.5″ and solar-Y = 12.6 to 29.3″). This area includes those regions which brighten in Ne vi in the subsequent rasters and where there are small brightenings in the lower temperature lines. We then measured the intensities over the same area in rasters 2, 3 and 4, allowing for solar rotation and small shifts in the location of the Ne vi emission. The differences in the intensity were then used to find the percentage increases over the intensities in raster 1. The intensities and differences are given in Table 3, and are illustrated in Fig. 6. (Since the intensities cannot be measured to better than ±5%, only changes of ≥7% are significant). The percentage increases do depend on the area assigned to the region that brightens, which has been matched to Ne vi. If the area that brightens in other emission lines occupies only n pixels^2 (n < 66), then the percentage increase within this smaller area will be underestimated by a factor of 66/n.

From Fig. 6 it can be seen that lines formed below T_e = 2.5×10^5 K (He i, He ii, O iii and O iv) increase fairly steadily by up to about 30%; Ne v increases in the second raster and then hardly varies; the Ne vi and Ne vii lines increase significantly in the second raster, and then decrease before increasing further. The increases in the O iii, O iv and O v lines are slightly smaller than the mean values in the blinkers discussed by Harrison et al. (1999) (28, 43 and 48%, respectively). The He i (584.3-Å) line increases by more than the average value of 8% reported by Harrison et al. (1999).

3.3. Line widths and shifts

We have investigated the profiles of the Ne vi (562.80-Å) and Ne vii (561.73-Å) lines in the region where the strongest brightening occured. Figure 7 shows the profiles of these lines in the four rasters, derived from the intensity summed over the region of the brightening. Simultaneous fits have been made to the profiles. Potential blends have been assessed using level populations and transition probabilities from the CHIANTI data base (Dere et al. 1997; Landi et al. 1999). The Ne vi line at 562.71 Å should contribute less than 10% of the total intensity around 562.80 Å. The Ne vii transition at 562.992 Å should have an intensity which is less than 2% that of the Ne vii line observed at 561.728 Å. Thus the 562.992-Å line should not influence the width or wavelength of the Ne vi line at 562.80 Å. The Ne vii line at 561.378 Å should have an intensity which is 20% that of the line at 561.728 Å, and will contribute to the measured line width; the Ne vii line is therefore not considered further.

We have compared the Ne vi line widths and wavelengths with those averaged over the whole quiet region to the north of that where the Ne vi and vii lines are enhanced (i.e. solar-$Y \geq +50''$). This avoids uncertainties in the wavelength calibration. In the quiet region the mean width ($FWHM$) of the Ne vi line is 0.48 ± 0.01 Å, essentially the same as the instrumental resolution which is expected to be ≃0.50 Å. In the region where the Ne vi line is enhanced, the width is not significantly broader, and has a mean value of 0.49 ± 0.01 Å. Because this width is so close to the instrumental resolution (defined by

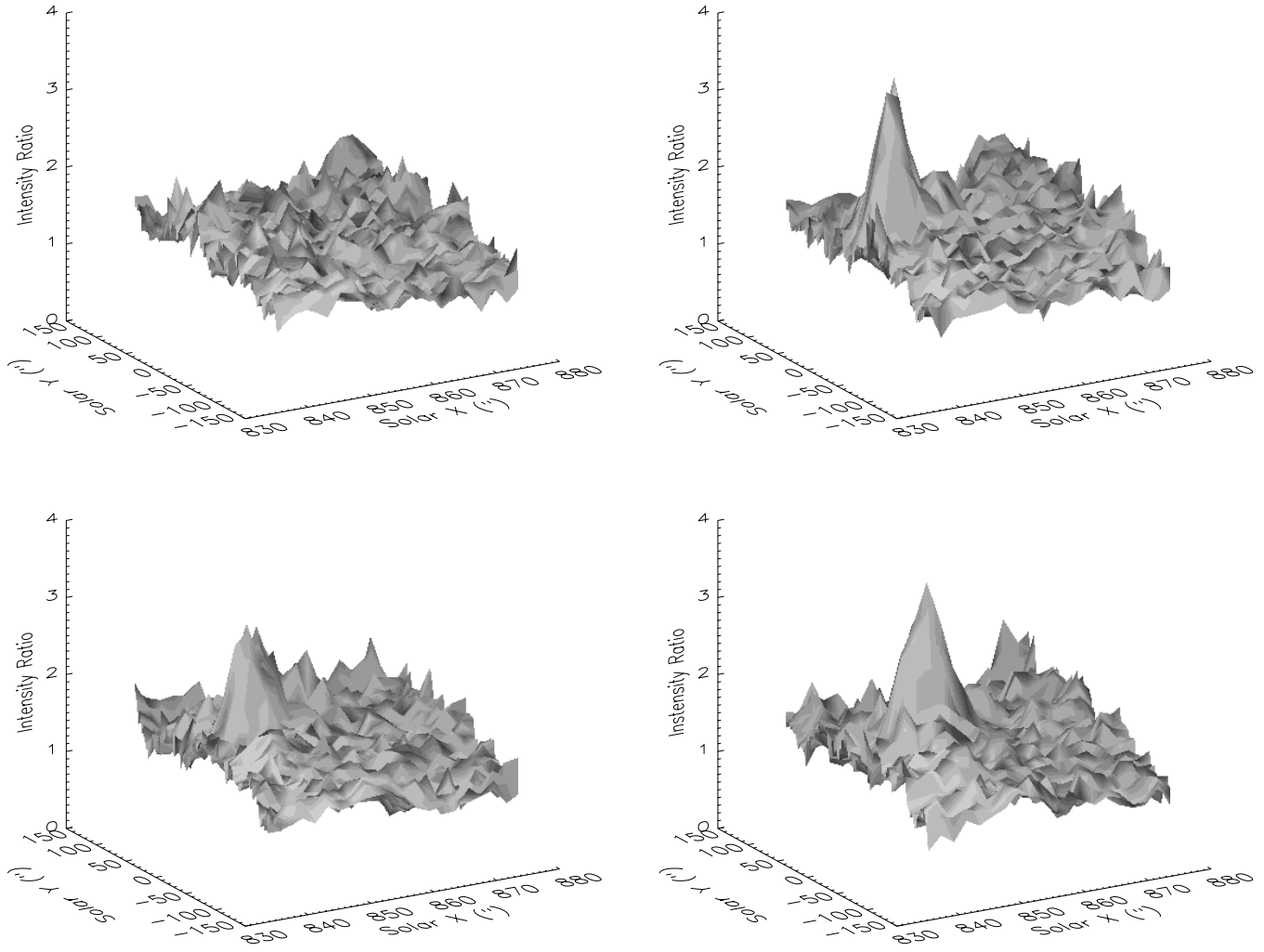

Fig. 5. The ratio of the Ne vi to Ne iv line intensities. In the first image, no significant feature appears above the noise level apart from a weak enhancement in the north-west. In the remaining images, the Ne vi brightening clearly stands out as a sharp enhancement in the ratio. Note that the background emission has not been removed in these images.

the quiet region value), the intrinsic, non-thermal width cannot be determined to any useful accuracy; any value of the most probable velocity up to $\simeq$100 km s^{-1} could be present.

During the transient event the Ne vi line is on average red-shifted by 12 km s^{-1}, relative to the quiet region, which is comparable to the combined measurement uncertainties. The wavelengths measured from the individual rasters agree with each other to within less than the mean shifts. Thus there are, at most, only small line-of-sight red shifts (relative to the quiet region) in the region where the Ne vi line is strong, and no evidence of blue-shifts. If the small changes in the location of the strongest emission are interpreted as motions transverse to the line of sight, velocities of only a few km s^{-1} result.

Table 3. Intensities (erg cm^{-2} s^{-1} sr^{-1}) in raster 1, integrated over 66 pixels^2, and excess intensities (over those in raster 1), in rasters 2, 3 and 4. No second order correction has been applied to the He ii line.

Spectral line	Raster 1	Raster 2	Raster 3	Raster 4
He i 584	57 710	3940	8220	17 740
He i 537	4310	980	1320	1040
He ii 304	12 020	−430	40	2760
O iii 599	4730	−90	310	950
O iv 554	30 400	2260	5290	7290
Ne iv 544	1030	220	250	200
O v 630	43 990	7150	13 200	13 400
Ne v 572	1130	690	760	640
Ne vi 563	2100	2200	1820	2450
Ne vii 562	910	400	150	670
Mg ix 368	51 730	890	660	−2370
Mg x 625	9870	360	760	−270

4. Interpretation

4.1. Possible geometry

The relatively low spatial resolution of the observations restricts any analyses which require knowledge of the geometry of the emitting region. However, on the basis of the information discussed below, at some stages we have assumed a loop geometry to explore the plasma conditions and energy balance. In the region where the Ne vi and Ne vii lines brighten there is

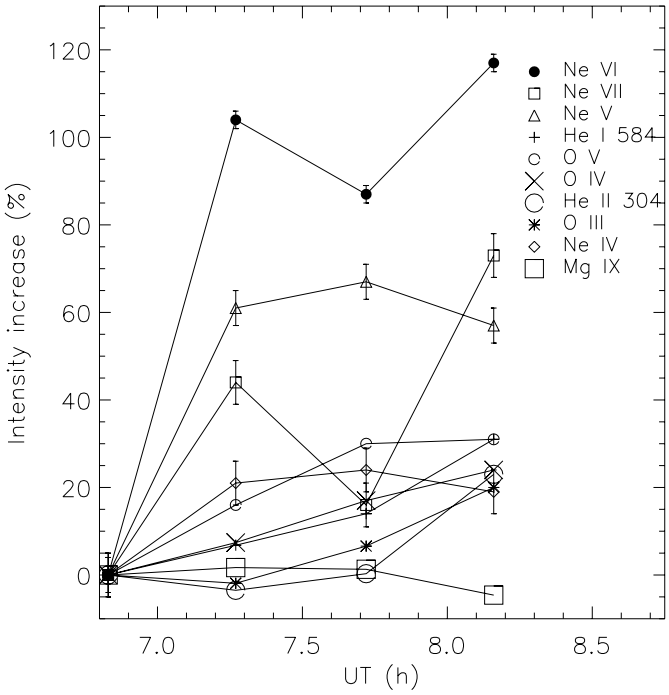

Fig. 6. Increases in the line intensities in rasters 2, 3 and 4, as a percentage of the intensities in the first raster, integrated over an area of 66 pixel^2.

no larger than average emission in the Mg x line, which typically represents emission from the inner corona. There is, however, a patch of stronger than average emission in the Mg ix line (see Fig. 1). We suggest that this Mg ix emission originates from relatively cool, small loop structures which are present throughout our observations. Using a more enhanced grey scale, there are no obvious *large scale* loop structures in which the strong Ne vi and vii emission would form only one footpoint.

We propose that the additional material emitting in Ne vi and vii exists within a loop (or loops) that is viewed more or less from above. This would produce the patch of emission observed in the images shown in Fig. 1. The changes apparent in Fig. 4, between rasters 3 and 1 and between rasters 4 and 1 could be occuring within the sides of one loop, or in different smaller loops. For simplicity we assume there is one loop. The maximum temperature in the loop is $\simeq 4-5 \times 10^5$ K, lower than that at which the Mg ix line is formed. No significant increase occurs in the weak Mg vii line (formed at $\simeq 6.3 \times 10^5$ K), which lies in the blue wing of the Mg ix line. In this model, the large Ne vi/Ne iv intensity ratios would occur because the loop is essentially isothermal at around $4-5 \times 10^5$ K, with the Ne iv emission originating from the separate underlying region.

4.2. Volume emission measures and electron pressures

The line intensities in raster 1 and the increases in the line intensities over those in raster 1 can be used to find the volume emission measures ($Em(V)$) of the original material and of the additional material during the brightening. Both refer to the *total* emission in the area defined in Sect. 3, and do *not* depend on any assumed geometry. Here $Em(V)$ is defined as $\int N_e^2 \, dV$, where the integral is taken over a range of $\Delta \log T_e = \pm 0.15$ about the optimum temperature for the line formation. We make use of the atomic data in the CHIANTI data-base (Dere et al. 1997; Landi et al. 1999) and adopt the relative ion populations of Arnaud & Rothenflug (1985).

Both oxygen and neon are elements with a high first ionization potential (FIP). We adopt the photospheric abundance of oxygen and the cosmic abundance of neon recommended by Grevesse et al. (1992). Magnesium is a low FIP element and might be subject to an abundance increase compared to the photospheric value. Young & Mason (1997 and see references therein) studied *active region* loops and found Mg/Ne relative abundances that varied between the "photospheric" value and nine times this value. However, there are no reported cases where the neon abundance is increased relative to magnesium. The ratios of the O iv and Ne iv line intensities are not significantly different from those measured at Sun centre, which led to the standard relative abundances (see Macpherson & Jordan 1999).

Using the excess intensities in raster 4, the emission measures found for Ne vi and Ne vii are 2.3×10^{43} cm^{-3} and 4.2×10^{43} cm^{-3}, respectively, over a range of $\Delta \log T_e = \pm 0.15$ about the optimum temperatures for the line formation given in Table 2. Allowing for the overlapping range of temperature covered by each line, summing the emission measures above $\log T_e = 5.10$ leads to total emission measures of 2.3×10^{43} cm^{-3}, 1.9×10^{43} cm^{-3} and 3.0×10^{43} cm^{-3}, for rasters 2, 3, and 4, respectively. The totals are dominated by the material above $\log T_e = 5.5$.

Rather than showing the volume emission measure distribution, in Fig. 8 we show the *changes* in the volume emission measures, as a function of $\log T_e$(K), relative to those from raster 1. These are given by $\log[(\Delta I(\text{line})/\Delta I(\text{O iv}))_n/(I(\text{line})/I(\text{O iv}))_1]$, where ΔI is the total intensity of the additional material and n is the raster number. The normalisation to O iv shows that most of the additional material occurs at the temperatures where the Ne v, vi and vii lines are formed. Ratios involving values of ΔI(line) that are not statistically significant are shown in parentheses. In this form of plot, the results are independent of the atomic data and of the total area observed. They do not depend on the absolute element abundances, but do assume that the relative abundances are constant with T_e. The lines of helium are not shown, since their intensities are controlled by complex enhancement processes which influence the temperatures at which they are excited (see Macpherson et al. 1999; Jordan et al. 2001; Smith & Jordan 2002). Their behaviour will be studied in future work.

There are no lines in our spectra which can be used to measure the electron density. The potentially useful line of O iv at 625.85 Å is not observed. The upper limit to this line intensity, combined with the intensity of the O iv line at 553.3 Å, leads to $N_e \leq 2.5 \times 10^{10}$ cm^{-3}, making use of Fig. 8 in Young & Mason (1997). The corresponding pressure ($P_e = N_e T_e$) is $\leq 4.7 \times 10^{15}$ cm^{-3} K. Thus the region is not one of exceptionally high density or pressure.

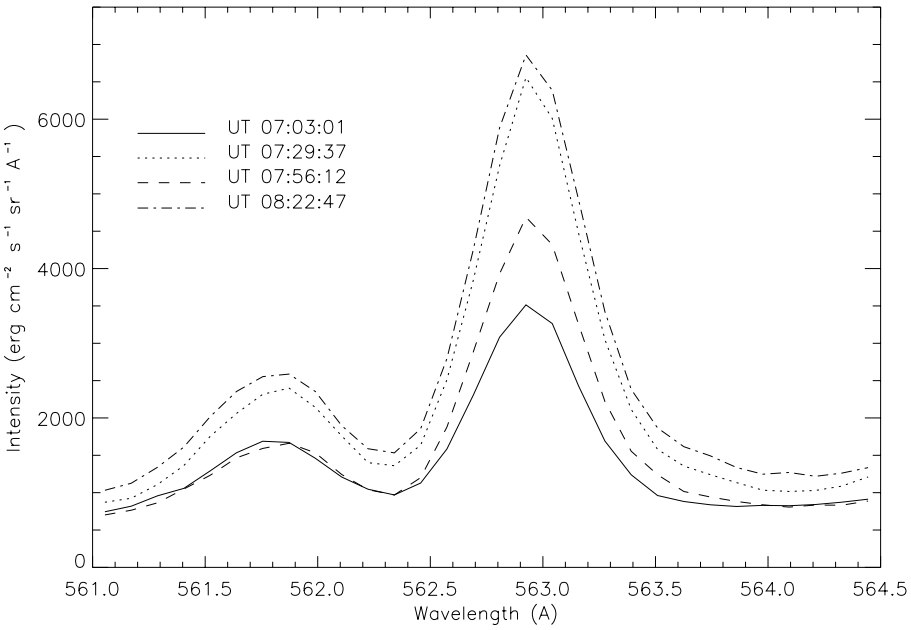

Fig. 7. The profiles of the Ne vi (562.80-Å) and Ne vii (561.728)-Å) lines in the four rasters, using intensities integrated over the region where the brightening in the Ne vi line is strongest. There are no significant changes in the profiles or line widths between the four rasters. The Ne vi and Ne vii lines are well separated and have been fitted simultaneously.

To estimate N_e, the geometry of the emission has to be used. The projected area of the emission can be measured, and hence line-of-sight emission measures ($\int N_e^2 dl$) can be found. At this point we assume that half of the photons created escape in the line of sight. To estimate N_e, a line of sight thickness through the region must also be assumed. If any loops present are close to isothermal in the lines of Ne vi and vii, then the minimum projected extent of the emission can be used as the line-of-sight thickness. Using a minimum diameter of 4 pixels in the X-direction (5800 km) and an extent in the Y-direction of 13 700 km, the spatially averaged values of N_e derived from rasters 2, 3 and 4 are 3.0×10^8 cm^{-3}, 2.7×10^8 cm^{-3} and 3.2×10^8 cm^{-3} (for Ne vi) and 3.3×10^8 cm^{-3}, 2.2×10^8 cm^{-3} and 5.0×10^8 cm^{-3} (for Ne vii). The mean pressures from Ne vi and vii are $P_e = 1.3\times10^{14}$ cm^{-3} K and 1.8×10^{14} cm^{-3} K, respectively. These pressures are similar to the mean values found for network boundary regions by Jordan et al. (2001) using density sensitive lines of C iii and N iii in sumer spectra (at the quiet Sun centre, 1.7×10^{14} cm^{-3} K; in a high latitude region outside a coronal hole, 2.2×10^{14} cm^{-3} K). However, if the observed structure is composed of smaller elements we cannot rule out higher pressures within them (and smaller pressures between them). E.g., if the emission occupied only a fraction f of the observed area, and the path length is scaled accordingly, the pressure in the area occupied will scale as $f^{-0.75}$.

4.3. Estimates of cooling times

To account for the increase in the radiation losses above $\simeq 2.5\times10^5$ K, some source of heating must have been present between rasters 1 and 2. We do not have sufficient information to estimate any heating or cooling from processes involving flows, but give simple estimates of the radiative and conductive cooling times in a static loop. Since changes in the mass present occur, in the longer term it would be of interest to make comparisons with the predictions of time-dependent models.

Adopting the above pressures, the radiative cooling times can be estimated. The radiative cooling time is given by

$$\tau_R = \frac{3}{P_e}\frac{k_B T_e^2}{P_{rad}(T_e)} \quad (1)$$

where $P_{rad}(T_e)$ is the radiative power loss function. We adopt values of $P_{rad}(T_e)$ from Cook et al. (1989), using photospheric and cosmic abundances as given above. Equation (1) then gives $\tau_R \simeq 30$ min, for both Ne vi and Ne vii. Higher pressures will result in shorter cooling times. Since the enhanced emission lasts for at least 53 min, some continued energy input is likely, but is not proven.

The conductive cooling time $3P_e k_B/(dF_C/dh)$, where F_C is the conductive flux), is hard to calculate with any accuracy. Using the simplest approximation (see e.g. van den Oord et al. 1988) for a loop of constant cross-section area,

$$\frac{dF_C}{dh} = \frac{\kappa T_e^{7/2}}{L^2} \quad (2)$$

where L is the half-length of the emission and $\kappa \simeq 10^{-6}$ erg cm^{-1} s^{-1} K$^{-7/2}$. This gives $\tau_C \simeq 8$ min, for Ne vi and $\simeq$4 min for Ne vii. Higher pressures will lead to longer cooling times. Although this method is very approximate, it does suggest that thermal conduction should be included.

The minimum energy input required can be estimated by summing the radiation losses. We use

$$\frac{dF_R}{dT_e} = 0.8 N_e^2 P_{rad}(T_e)\frac{dh}{dT_e}. \quad (3)$$

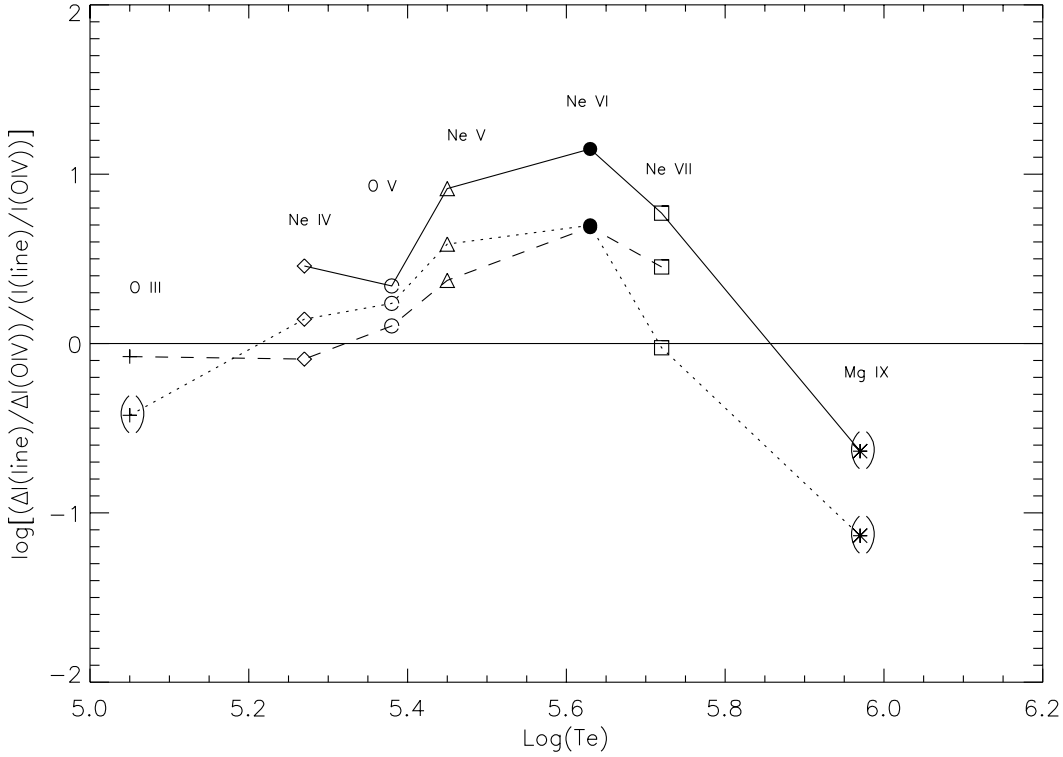

Fig. 8. The values of $\log[(\Delta I(\text{line})/\Delta I(\text{O IV}))_n/(I(\text{line})/I(\text{O IV}))_1]$ where ΔI is the total intensity of the additional material and n is the raster number, as a function of $\log T_e$(K). Full line, raster 2; dotted line, raster 3; dashed line, raster 4. These ratios give the fractional changes in $Em(V)$, normalised to the fractional change in $Em(V)$ for the O IV line. Most of the additional material occurs at temperatures where the Ne v, Ne VI and Ne VII lines are formed. Ratios involving ΔI that are not statistically significant are shown in parentheses.

The temperature gradient can be written in terms of the height emission measure (again, for the range $\Delta \log T_e = \pm 0.15$ about the optimum temperature of line formation), using

$$Em(0.3) = \frac{Em(V)}{2A} = \frac{P_e^2}{\sqrt{2}T_e}\frac{dh}{dT_e} \quad (4)$$

where A is the assumed cross-sectional area of the loop. The radiative flux from a chosen logarithmic temperature range is then

$$\Delta F_R = 2.7 P_{rad}(T_e)\frac{Em(V)}{2A}\Delta \log T_e. \quad (5)$$

The radiation losses can then be summed and have values of $\simeq 1.0 \times 10^5$ (raster 3) to 1.4×10^5 erg cm^{-2} s^{-1} (raster 4), for each half of the loop.

The conductive flux leaving each half of the loop at $T_e = 2 \times 10^5$ K can also be estimated from

$$F_C = -\kappa T_e^{5/2}\frac{dT_e}{dh}. \quad (6)$$

Using Eq. (4) for dT_e/dh and the volume emission measures for O IV and the pressures derived above, leads to values of F_C that range from 1.6×10^5 (raster 1) to 5.6×10^4 erg cm^{-2} s^{-1} (raster 4). The total energy flux required is $\simeq 2 \times 10^5$ erg cm^{-2} s^{-1} in all three rasters. This is at least a factor of 3 lower than the average for the mean corona, which is not surprising, given that the maximum temperature in the loop is lower.

4.4. The nature of the event

It is possible that the event observed is an unusually large blinker which reaches a higher than average temperature. As in blinkers, the increases in the He I 584.3-Å and Mg IX line are small. Since observations of blinkers have not previously included lines which are formed at temperatures between $\simeq 2.4 \times 10^5$ K (corresponding to O V) and $\simeq 9.3 \times 10^5$ K (corresponding to Mg IX), such events may have been overlooked. The size and duration of the event are at the high end of those for blinkers, but the intensity increases are not dissimilar.

It has been suggested that blinkers result from magnetic reconnection when small loops of magnetic flux interact with the network fields (Harrison et al. 1999). These may be structures swept to the boundaries by the convective flow, or newly emerged flux; in either case new material could be injected during the reconnection process. However, the emergence of new magnetic flux need not involve reconnection, since the material could be heated in situ by MHD waves. Similarly, if new material is pushed up an existing flux tube, this could be heated in situ. At present, the lack of accurate line width and line shift measurements prevents us from distinguishing between these alternatives. In studies with SUMER, the hottest line used in studies of blinkers has been a S VI line, formed (like O IV and Ne IV) at around 2×10^5 K (Madjarska & Doyle 2002). It would be worth while extending such work to include lines formed at higher temperatures, since only SUMER has the necessary spectral resolution to measure accurate line widths and shifts.

The event does not appear to be an explosive event. According to Brueckner & Bartoe (1983), explosive (turbulent) events are observed *simultaneously* in transition region lines formed between temperatures of $\simeq 2 \times 10^4$ K (the C II lines) and $\simeq 2 \times 10^5$ K (the N v lines). The event we observe does not fit this behaviour, since it shows only very small increases in lines formed at temperatures formed below $\simeq 2 \times 10^5$ K. Also, the turbulent events observed by Brueckner & Bartoe (1983) are confined to very small areas ($\leq$4 arcsec) and exist for short times ($\leq$6 min) (Dere 1994), although some events do re-occur at the same location over a period of up to 30 min (Chae et al. 1998).

The event involves the addition of new material, either in the form of a new flux tube, or as material added to an existing flux tube. In either case the material is initially heated to about the temperature at which Ne VII is formed. The new material does not appear to arise through the cooling of hotter material, since the Mg IX intensity does not show statistically significant decreases, and in fact shows very small increases in rasters 2 and 3. Because some structure is already present in Mg IX (and the Mg X line is relatively weak) it is possible that mass has been injected into a loop (or set of loops) which is cooler than the temperature at which Mg IX is formed.

The mass in the region over which a line is formed can be found from $Em(V)$ and N_e. Using the full emission measure distribution for mean boundary regions from Macpherson et al. (1999), and our estimated densities, in order to obtain a sufficient increase in mass at $\simeq 5 \times 10^5$ K by heating existing material would require this material to be at an original temperature below 3×10^4 K. At such low temperatures the mass per unit temperature range is high enough to lead to only small decreases in the line intensities. At and above the optimum temperatures for line formation, the ionisation times for the oxygen and neon ions observed are all short (2–10 min), so with our exposure times and raster cadence one would not expect to see a successive brightening in lines formed at increasing temperatures. However, with sufficient time resolution, if the above situation occurs, one should observe up to an order of magnitude increase in lines formed at around $1\text{–}2 \times 10^5$ K, as the increase in mass passed through these temperatures, where the normal mass per unit temperature range is smaller. Many studies of *active region* loops have shown time variable behaviour in transition region lines (see Fredvik et al. 2002 and references therein) and the associated theory of loop stability has been discussed by Priest (1981). It may therefore not be surprising if loops associated with supergranulation boundary regions show a similar behaviour.

5. Conclusions

We have observed an unusual transient event which is strongest in the lines of Ne v, Ne VI and Ne VII. The main increase in the volume emission measure therefore takes place over the temperature range 3×10^5 K to 5×10^5 K. The Ne IV/O IV intensity ratio is similar to that in the average network, suggesting that changes in relative abundances are not the cause of the high intensities in the hotter lines of neon. There is no evidence for an unusually high electron pressure in the region ($P_e \leq 5 \times 10^{15}$ cm^{-3} K); we estimate $P_e \simeq 1 - 2 \times 10^{14}$ cm^{-3} K, similar to values found for the normal network (Macpherson & Jordan 1999; Jordan et al. 2001). The total apparent volume emission measure reaches 3.0×10^{43} cm^{-3}. The total energy flux required is $\simeq 2 \times 10^5$ erg cm^{-2} s^{-1}, about half of which is due to radiation losses. The event clearly involves an increase in the mass present over the above temperature range. This increase does not appear to be balanced by a decrease in mass at higher temperatures. The injection of mass into a previously existing cool loop is a possible explanation for the event.

The event shares some characteristics with blinkers, such as small increases in the lines of He I and Mg IX, although its extent and duration are larger than average for blinkers. It does not appear to be an explosive event or network flare, on the basis of the relative behaviour of the transition region lines. Although the cadence of our 4 sets of rasters is not ideal for studies of blinkers we *can* say the the large majority of small network brightenings which appear in the lines of O III, O IV, Ne IV and O V do also show up in the hotter lines of neon. While previous observations of blinkers would not have shown the event we observe, our data sets show only one other obvious example of high Ne VI to O IV and O V ratios. In this respect the observed event is clearly unusual. Future studies of blinkers need to include lines formed over the full range of temperatures between the low transition region and corona.

Acknowledgements. SOHO is a cooperative mission between ESA and NASA. We thank the CDS instrument team and science planner for assistance in designing and implementing the observing sequence used and the EIT team for access to their data. ERH would like to thank Dr. D. Pike for helpful assistance in using the CDS software. We are grateful to the referee, Dr. H. Peter, for useful suggestions which improved the paper. This work was supported by PPARC Grant PPA/G/S/2000/00076.

References

Allen, C. W. 1973, Astrophysical Quantities, Third edn. (London: Athlone Press)
Arnaud, M., & Rothenflug, R. 1985, A&AS, 60, 425
Benz, A. O., & Krucker, S. 1998, Sol. Phys., 182, 349
Berghmans, D., Clette, F., & Moses, D. 1998, A&A, 336, 1039
Brekke, P., Thompson, W. T., Woods, T. N., & Eparvier, F. G. 2000, ApJ, 536, 959
Brković, A., Solanki, S. K., & Rüedi, I. 2001, A&A, 373, 1056
Bromage, B. J. I., Breeveld, A. A., Kent, B. J., Pike, C. D., & Harrison, R. A. 1996, Univ. Central Lancashire Report CFA/96/09
Brueckner, G. E., & Bartoe, J.-D. F. 1983, ApJ, 272, 329
Chae, J., Wang, H., Lee, C. Y., Goode, P. R., & Schühle, U. 1998, ApJ, 497, L109
Chae, J., Wang, H., Goode, P. R., Fludra, A., & Schühle, U. 2000, ApJ, 528, L119
Cook, J. W., Cheng, C.-C., Jacob, V. L., & Antiochos, S. K. 1989, ApJ, 338, 1176
Dere, K. P. 1994, Adv. Space Res., 14, 13
Dere, K. P., Landi, E., Mason, H. E., & Monsignori-Fossi, B. C. 1997, A&AS, 125, 149
Domingo, V., Fleck, B., & Poland, A. I. 1995, Sol. Phys., 162, 1
Fredvik, T., Kjeldseth-Moe, O., Haugan S. V. H., et al. 2002, Adv. Space Res., 30, 635

Grevesse, N., Noels, A., & Sauval, A. J., 1992, in ESA SP-348, Coronal Streamers, Coronal Loops, and Coronal and Solar Wind Composition, ed. C. Mattock (Noordwijk: ESA Publications Division), 141
Harrison, R. A., 1997, Sol. Phys., 175, 467
Harrison, R. A., Lang, J., Brooks, D. H., & Innes, D. E. 1999, A&A, 351, 1115
Harrison, R. A., Sawyer, E. C., Carter, M. K., et al. 1995, Sol. Phys., 162, 233
Jordan, C. 2000, Plasma Phys. Controlled Fusion, 42, 415
Jordan, C., Macpherson, K. P., & Smith, G. R. 2001, MNRAS, 328, 1098
Kelly, R. L. 1987, J. Phys. Chem. Ref. Data, 16, Suppl. No. 1
Krucker, S., Benz, A., Acton, L. W., & Bastian, T. S. 1997, ApJ, 488, 499
Landi, E., Landini, M., Pike, C. D., & Mason, H. 1997, Sol. Phys., 175, 553
Landi, E., Landini, M., Dere, K. P, Young, P. R., & Mason, H. E. 1999, A&AS, 135, 339
Macpherson, K. P., & Jordan, C. 1999, MNRAS, 308, 510
Madjarska, M. S., & Doyle, J. G. 2002, A&A, 382, 319
Priest, E. R. 1981, in Solar Active Regions, ed. F. Q. Orrall (Boulder: Colorado Assoc. Univ. Press), 213
Smith, G. R., & Jordan, C. 2002, MNRAS, 337, 666
Teriaca, L., Madjarska, M. S., & Doyle, J. G. 2001, Sol. Phys., 200, 91
van den Oord, G. H. J., Mewe, R., & Brinkman, A. C. 1988, A&A, 205, 181
Winebarger, A. R., Emslie, A. G., Mariska, J. T., & Warren, H. P. 2002, ApJ, 565, 1298
Young, P. R., & Mason, H. E. 1997, Sol. Phys., 175, 523